the radial velocity fluctuations were considerably attenuated because the 180-μm particles could not follow the high frequencies involved in the radial velocity fluctuations.

References

[1]Al Taweel, A. M., and Landau, J., "Turbulence Modulation in Two-Phase Jets," *International Journal of Multiphase Flow*, Vol. 3, No. 2, 1977, pp. 341–351.

[2]Gore, R. A., and Crowe, C. T., "Effects of Particle Size on Modulating Turbulent Intensity," *International Journal of Multiphase Flow*, Vol. 15, No. 2, 1989, pp. 279–285.

[3]Schreck, S., and Kleis, S. J., "Modification of Grid-Generated Turbulence by Solid Particles," *Journal of Fluid Mechanics*, Vol. 249, 1993, pp. 665–688.

[4]Kulick, J. D., Fessler, J. R., and Eaton, J. K., "Particle Response and Turbulence Modification in Fully Developed Channel Flow," *Journal Fluid Mechanics*, Vol. 277, 1994, pp. 109–134.

[5]Sato, Y., Hishida, K., and Maeda, M., "Effect of Dispersed Phase on Modification of Turbulent Flow in a Wall Jet," *Journal of Fluids Engineering*, Vol. 118, No. 2, 1996, pp. 307–315.

[6]Chang, Y.-H., "Velocity Measurements in a Particle-Laden Round Jet Using Discriminator Laser Doppler Velocimetry," M.S. Thesis, School of Aerospace and Mechanical Engineering, Univ. of Oklahoma, Norman, OK, Jan. 1998.

[7]Parthasarathy, R. N., and Faeth, G. M., "Structure of Particle-Laden Turbulent Water Jets in Still Water," *International Journal of Multiphase Flow*, Vol. 13, No. 5, 1987, pp. 699–716.

[8]Muste, M., Parthasarathy, R. N., and Patel, V. C., "Discriminator Laser Doppler Velocimetry for Measurement of Liquid and Particle Velocities in Sediment-Laden Flows," *Experiments in Fluids*, Vol. 22, No. 1, 1996, pp. 45–56.

[9]Ahmed, S. A., Nejad, A. S., and Al-Garni, A. Z., "A Comparative Study of the Effects of LDV Velocity Bias in the Near Field of a Turbulent Free Jet," *Canadian Aeronautics and Space Journal*, Vol. 41, No. 4, 1995, pp. 179–184.

[10]Hussein, J. H., Capp, S. P., and George, W. K., "Velocity Measurements in a High-Reynolds-Number Momentum-Conserving, Axisymmetric, Turbulent Jet," *Journal of Fluid Mechanics*, Vol. 258, 1994, pp. 31–75.

A. K. Aggarwal
Associate Editor

Evolution Strategies for Film Cooling Optimization

Sibylle D. Müller,* Jens H. Walther,†
and Petros D. Koumoutsakos‡
*Swiss Federal Institute of Technology, ETH Zentrum,
8092 Zurich, Switzerland*

Introduction

AN evolutionary algorithm is implemented in a realistic automated design cycle of turbine blade film cooling. This design cycle involves the use of empirical formulas for the flow calculation and the use of a commercial software package for the simulation of the heat transfer problem. The overall process consists of an engineering multiobjective optimization problem with constraints. In this work we consider the solution of this problem in the context of an automated optimization cycle using evolution strategies. Evolution strategies[1] are robust, highly parallelizable, and suitable for optimizing multimodal functions without requiring gradient information. An evolution strategy with derandomized covariance matrix adaptation of the mutation distribution is chosen that accelerates the convergence rate of the scheme by adaptively incorporating earlier information.[2] It is shown to be advantageous in this problem when compared with an evolution strategy with isotropic mutation distribution and cumulative global step size adaptation. In film cooling,
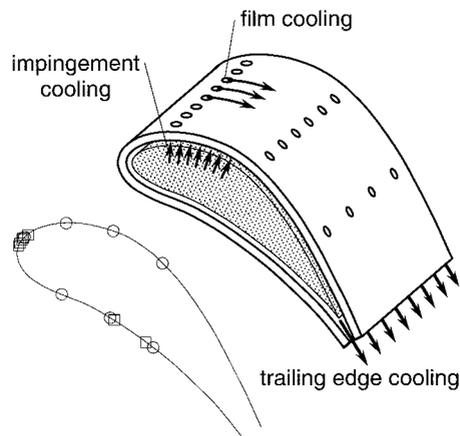
*Graduate Student, Institute of Computational Sciences.
†Research Associate, Institute of Computational Sciences.
‡Professor, Institute of Computational Sciences.

Fig. 1   Three cooling mechanisms and the initial (○) and final (□) row positions from the optimization with the CMA–ES.

the coolant leaves the blade through rows of holes, forming a protective film on the outer surface of the blade, separating the hot gas from the metal. The design of the cooling configuration aims at both minimizing the coolant supply and achieving optimum cooling, while obeying certain engineering constraints. For the simulation of the cooling configuration, we compute the mass flow of the coolant and the surface temperature of the blade based on given external aerodynamic and thermal conditions for a two-dimensional blade geometry.

Description of a Blade Cooling Configuration

A typical vane cooling configuration is shown in Fig. 1. It consists of three components: 1) an insert for impingement cooling, 2) the trailing-edge geometry for convection cooling, and 3) coolant air leaving the inside of the blade through holes and keeping attached as a film, thereby cooling the outer surface. The coolant flow is described by three different cooling mechanisms based on empirical correlations that compute the heat transfer coefficient and the temperature in the boundary layer.[3–5] The geometry and the external aerodynamic and thermal conditions are considered two dimensional, and the shape of the blade is fixed.

Blade Cooling Optimization

Optimization Algorithm and Parameters

The two chosen optimization techniques[2] are evolution strategies with intermediate recombination of all of the parents and with a population of 3 parents and 12 children, using strategy parameters according to Ref. 2. The first method is an evolution strategy with derandomized covariance matrix adaptation (CMA–ES), whereas the second method is an evolution strategy with isotropic mutation distribution and cumulative global step size adaptation (ES).

The optimization parameters are the number of film cooling rows R_f; the position of film cooling rows $s_{pos}(1-R_f)$; the injection angles of the holes, measured from the hole axis to the surface $\alpha(1-R_f)$; the number of holes per row $N_r(1-R_f)$; the number of impingement holes N_j; and the loss parameter that is a function of the pressure loss in the trailing edge A_{loss}.

The only integer parameter in the blade cooling optimization is the number of rows. Note that optimizing integer variables with an ES only makes sense if the number of possibilities to adjust the variables is large enough. Because of manufacturing requirements, the number of rows should not exceed about 10. With respect to this small number, this parameter is not included in the optimization process, but rather is changed manually for different optimization runs. First tries with $R_f = 4$ showed that the constraints for maximum and minimum temperature cannot be met. To homogenize the temperature distribution, we increased the number of rows to $R_f = 7$. This number was found to be sufficient for achieving the optimization goals and is used in this study.

All of the other parameters are real valued. For each film row $j = 1, \ldots, R_f$, the position s_{pos}, the angle α, and the number of holes per row N_r can be chosen. The other two parameters are the

number of impingement holes N_j and the loss parameter A_{loss}. There are $3 \times R_f + 2$ parameters altogether, in our case 23 parameters.

The limits of the optimization parameters are set to $0 \leq s_{pos} \leq 1$, $30 \leq \alpha \leq 90$ deg, $10 \leq N_r \leq 100$, $500 \leq N_j \leq 1000$, $1 \leq A_{loss} \leq 3$. The parameter range of s_{pos} covers the whole surface starting from $s_{pos} = 0$ at the trailing edge, continuing on the suction side to the stagnation point, and on the pressure side back to the trailing edge. For the angle α, a special constraint is imposed by engineering considerations. In the leading edge of the blade, defined by values of s_{pos} between 0.49 and 0.53, holes with angles other than 90 deg are difficult to manufacture due to the high curvature. Therefore, holes in the leading-edge region should always be set to 90 deg. This is a constraint that can be neglected for the following reason: In all of the optimization runs, the objective function values are not sensitive to changes of the hole angles. This indicates that the influence of the injection angle is not sufficiently incorporated in the model. Instead of the constraint, we compare the outputs of the converged solution with the outputs computed with angles of 90 deg for rows of holes in the leading edge. For all of our optimization runs, the difference between both outputs was below 1%.

Objective Function

The main goal of the optimization is to minimize the mass flow of the coolant, $\dot{m}_c$. At the same time, constraints have to be met. These constraints are expressed by one equality constraint $\varepsilon_{mean} = 0.5$, where ε_{mean} is the normalized mean surface temperature, and also by the two inequality constraints $\varepsilon_{max} \leq 0.6$ and $\varepsilon_{min} \geq 0.4$, where ε_{max} is a function of the minimum temperature at the outer surface and where ε_{min} is a function of the maximum temperature. These constraints are incorporated in the objective function f using a distance method with Euclidean metric:

$$f = \left(\sum_{i=1}^{4} f_i^2 \right)^{0.5}$$

where $f_1 = \dot{m}_c$, $f_2 = |\varepsilon_{mean} - 0.5|/0.5$, and

$$f_3 = \begin{cases} 10{,}000 \times (\varepsilon_{max} - 0.5)^4 & \text{if } \varepsilon_{max} \geq 0.5 \\ 0 & \text{if } \varepsilon_{max} < 0.5 \end{cases}$$

$$f_4 = \begin{cases} 10{,}000 \times (\varepsilon_{min} - 0.5)^4 & \text{if } \varepsilon_{min} \leq 0.5 \\ 0 & \text{if } \varepsilon_{min} > 0.5 \end{cases}$$

The coefficients and the exponent can be considered weights and are chosen such that the functions f_3 and f_4 are larger than f_1 and f_2 for the initial parameters.

The computation of the optimization objectives entails two steps: The mass flow of the coolant and the air temperatures and heat transfer coefficients in the boundary layer as a function of the geometry have to be computed first. In a second step, the steady heat equation is solved for the unknown temperature distribution using second-order finite volume techniques subject to the aforementioned boundary conditions. The blade geometry is discretized using 660×20 mesh points, and the solution is obtained applying a commercial package, STAR-CD.[6] One function evaluation is done in about 15 CPU seconds on a Sun Ultra 60/Creator 3D, 300 MHz.

Results

With the initial parameter configuration $s_{pos} = (0.2, 0.3, 0.4, 0.5, 0.6, 0.7, 0.8)$, $\alpha = 50$ deg, $N_r = 50$, $N_j = 800$, and $A_{loss} = 2$, we obtain the objectives $\dot{m}_c = 0.367$, $\varepsilon_{mean} = 0.522$, $\varepsilon_{max} = 0.616$, $\varepsilon_{min} = 0.360$, and $f = 4.22$.

A reduction of the initial objective function value by 60% is achieved with the CMA–ES after about 200 generations (=2400 function evaluations). After about 1800 generations (=21,600 function evaluations), convergence is reached.

The optimum parameters $s_{pos} = (0.490, 0.500, 0.502, 0.508, 0.510, 0.706, 0.786)$, $\alpha = (65, 90, 89, 30, 30, 73, 30$ deg$)$, $N_r = (100, 10, 13, 95, 100, 35, 41)$, $N_j = 501$, and $A_{loss} = 2.97$ yield the outputs $\dot{m}_c = 0.257$, $\varepsilon_{mean} = 0.502$, $\varepsilon_{max} = 0.595$, $\varepsilon_{min} = 0.400$, and $f = 0.229$. Here, the reduction of the cost function equals 95%.
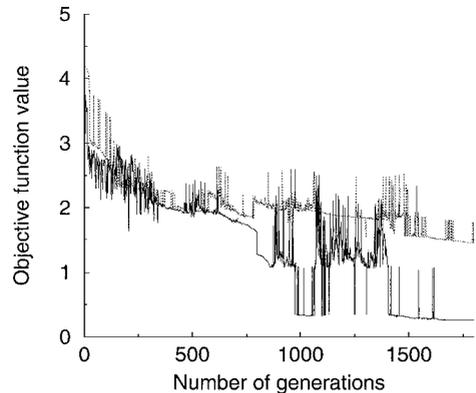

Fig. 2 Convergence of the objective function f: ——, CMA–ES and $\cdots$, ES.

The results of this study are summarized as follows: 1) The original row configuration (rows equidistantly placed) was drastically modified. The final configuration suggests to place five rows in the leading edge and two rows on the pressure side, as seen in Fig. 1. The number of holes per row attains small values for the rows on the pressure side, whereas two rows in the leading edge are equal to the upper limit, $N_r = 100$. This result makes sense when considering that the hot gas is approaching the leading edge of the blade, thus requiring efficient cooling in this area. 2) The mass flow can be reduced significantly, and the mean temperature distribution comes closer to the desired one. At the same time, the maximum and minimum temperatures are not exceeded, as seen from the constraints $\varepsilon_{max} < 0.6$ and $\varepsilon_{min} \geq 0.4$ that are met. 3) As can be seen from Fig. 2, where the improvement of the multiobjective function is shown, convergence is reached after about 1800 generations (=21,600 function evaluations in a population with 12 offspring) for the ES with CMA. Convergence is defined as reached when the difference of the cost function for the best individual is less than 10^{-3} (in absolute values) over 10 generations. On the other hand, the ES converges slower and cannot reach the same good value as the CMA–ES within the same number of iterations. The difference in convergence properties of these two types of evolution strategies agrees well with results from the optimization of several test functions.[2] 4) Although evolution strategies are often considered good candidates for global optimization, they may also converge to local optima. Therefore, to find a good optimum, it is recommended to perform several optimization runs with different start configurations. Because the computations in our case are relatively expensive, we optimized with only two different initial settings of the strategy parameters. The converged function values in both optimization runs did not significantly (1–2%) differ from each other. The final model parameters were not the same, but they represented a very similar configuration with five rows close to each other in the leading-edge region and two rows of holes on the pressure side.

When interpreting the results, one should keep in mind that we use an empirical model that may not take into full account the properties of the flow and heat problem. Moreover, the results could be improved by replacing the combination of the several objectives into one single objective function by searching the Pareto front of the multiobjective problem.

Conclusions

We presented results from the application of an improved parallel evolution strategy to the multiobjective optimization of parameters in a model of gas turbine blade film cooling with seven rows. The optimization goals were to reduce the coolant mass flow and at the same time achieve a homogenous surface temperature while observing certain constraints in the range of the temperature distribution. Starting from a number of initial configurations, the optimization algorithm was always able to produce a number of improved designs. The results of the present study suggest that evolution algorithms present a robust, automated optimization tool offering a viable alternative to the optimization of engineering devices using gradient-based methods and engineering intuition.

Acknowledgments

References

[1]Schwefel, H.-P., *Evolution and Optimum Seeking*, Wiley, New York, 1995, pp. 105–164.

[2]Hansen, N., and Ostermeier, A., "Convergence Properties of Evolution Strategies with the Derandomized Covariance Matrix Adaptation: The $(\mu/\mu_I, \lambda)$-CMA-ES," *Proceedings of the 5th European Congress on Intelligent Techniques and Soft Computing (EUFIT'97)*, Verlag Mainz, Aachen, Germany, 1997, pp. 650–654.

[3]McGreehan, W. F., and Schotsch, M. J., "Flow Characteristics of Long Orifices with Rotation and Corner Radiusing," American Society of Mechanical Engineers, ASME Paper 87-GT-162, June 1987.

[4]Goldstein, R. J., "Film Cooling," *Advances in Heat Transfer*, Vol. 7, 1971, pp. 321–379.

[5]Seller, J. P., "Gaseous Film Cooling with Multiple Ejection Stations," *AIAA Journal*, Vol. 1, No. 9, 1963, pp. 2154–2156.

[6]STAR-CD User Manual, Computational Dynamics, Ltd., London, Dec. 1997.

A. Chattopadhyay
Associate Editor

Role of Tip and Edge Geometry on Vortex Asymmetry

T. T. Lim,* K. B. Lua,† and S. C. Luo*
National University of Singapore, Singapore 119260, Republic of Singapore

Introduction

IN the late 1960s, Bird[1] investigated the flow over a delta wing at high incidence and noted the asymmetric lifting of the apex or tip vortices from the wing. However, a similar and more recent investigation by Stahl et al.[2] found the corresponding vortices to be symmetrical instead. Stahl et al.[2] and Ericsson[3] attributed the conflicting results to the different tip conditions of the two delta wings. They pointed out that the delta wing of Stahl et al.[2] had a triangular tip with sharp edges, whereas the one used by Bird[1] had a conical tip, which presumably was subjected to the same source of vortex asymmetry as an ogive–cylinder or a cone. The preceding explanation implies that the nose geometry plays a crucial role in determining the orientation of the tip vortices. To determine whether this is also true for other slender plates, we perform a series of flow visualization studies on an ogive-shaped plate at a high angle of attack. As the name implies, the plate has the same profile as the center plane of an ogive–cylinder in much the same way that a delta wing has the same profile as the center plane of an axisymmetric cone. This particular geometry is chosen for study because, apart from addressing the issue of vortex asymmetry, it enables comparison with previous experimental studies of the ogive–cylinder.[4,5]

Experimental Apparatus and Procedures

The experiments were performed in the National University of Singapore's 0.4×0.4 m test section water channel using a dye

*Associate Professor, Department of Mechanical and Production Engineering, 10 Kent Ridge Crescent.

†Research Engineer, Department of Mechanical and Production Engineering, 10 Kent Ridge Crescent.

visualization technique. A total of four ogive-shaped plates were fabricated, with different tip and edge conditions. All of the plates are 24 mm (D) wide and 3 mm thick and have the same tip finess ratio, that is, $3.5D$, as the ogive–cylinder used in our earlier study (Fig. 1a). In the first plate or model, the edges were chamfered at 45 deg and extended all of the way to the apex of the model. For ease of reference, it is referred to as sharp tip and sharp edges (STSE) (Fig. 1b). This model has the same tip and edge conditions as the delta wing used by Stahl et al.[2] In the second model, the edges were also chamfered, but the apex has an axisymmetric ogive tip of length 5.27 mm (or $0.22D$) (Fig. 1c). This model is referred to as ogive tip and sharp edges (OTSE). The third model has the same ogive tip as the OTSE model, but the edges are rounded with a radius of 1.5 mm (half of the model thickness) (Fig. 1d). This model is referred to as ogive tip and round edges (OTRE) and is the counterpart of the delta wing of Bird.[1] The last model has the same apex geometry as STSE and the round edges of OTRE. Accordingly, it is referred to as sharp tip and round edges (STRE) (Fig. 1e). These four models provide all of the possible combinations of sharp and rounded edge and tip geometries.

In the actual experiment, the base of each ogive-shaped plate was supported by a mechanism above the water surface, and the plate pitched downward and pierced through the free surface. This arrangement allowed the tip of the plate to be farthest away from the free surface, hence ensuring that free surface effects, if any, were kept to a minimum. Before each run, a height gauge was used to align painstakingly the model with the centerline of the test section and ensure that the yaw and roll angles were zero with respect to the freestream. This laborious process was deemed necessary because the accuracy of the results depended critically on the accuracy of the model alignment. To visualize the flow, dye was released slowly and with minimum disturbance to the flow from the two dye ports located at 20 mm from the apex and slightly on the leeward side of the model. In all cases, the groove that carries the stainless tubing for the dye injection was filled with epoxy resin and carefully shaped to match the profile of the body. For the purpose of distinguishing the two tip vortices, red dye was released from the port side of the model, and blue dye was released from the mirror image port on the starboard side. The operating Reynolds number based on the width of the plate was approximately 3.2×10^3.

The flow patterns were captured from the bottom and side of the test section using two charge-coupled device (CCD) video cameras and a Nikon F3 single-lens-reflex still camera equipped with a Nikkor 50-mm lens. To avoid the effect of parallax, extreme care was taken when aligning the camera with respect to the model. To conform with the common practice of flow direction from left to right, the side views of the captured images have been rotated by 180 deg, as shown in Figs. 2 and 3.

Results and Discussion

In Fig. 2, the side and the plan views of the tip vortices for the four ogive-shaped plates tested are displayed. Although the plates were tested for a range of moderately high angles of attack α from 40 to 60 deg, only the results for $\alpha = 40$ deg are presented because the salient flow features for the other angles are essentially the same.

Figure 2a shows the results for the STSE plate at $\alpha = 40$ deg. It is obvious from the dye patterns that the tip vortices were symmetrical up to the locations of the apparent vortex breakdown. The existence of the vortex breakdown is supported by the video images, which clearly show a region of recirculating flow immediately after the dye core has undergone sudden enlargement. It is not clear what caused the vortices to breakdown at the different positions, but a similar phenomenon has often been observed on the tip vortices from delta wings at high angles of attack.[2]

In Fig. 2b, the results for OTSE model are displayed. Here, it can be seen that the vortices remained symmetrical up to the vortex breakdown positions despite the model having an axisymmetric tip. This flow behavior is contrary to the speculation by Stahl et al.[2] and Ericcson,[3] which suggested that the vortices should be asymmetric if the tip is rounded. That the vortices were not asymmetric indicated that the axisymmetric tip may not be solely responsible for the vortex asymmetry. The sharp edges may have played an equally influential